

JGR Space Physics

RESEARCH ARTICLE

10.1029/2020JA028940

Special Section:

Solar and Heliospheric Plasma Structures: Waves, Turbulence, and Dissipation

This article is a companion to Verniero et al. (2021), <https://doi.org/10.1029/2020JA028361>.

Key Points:

- We develop a new algorithm, Particle Arrival Time Correlation for Heliophysics (PATCH), to quantify wave-particle energy transfer onboard spacecraft
- We qualitatively assess how PATCH can resolve the velocity-space signature of ion Landau damping
- We quantify the error of the PATCH method as the particle count rate varies

Correspondence to:

J. L. Verniero,
jlvverno@berkeley.edu

Citation:

Verniero, J. L., Howes, G. G., Stewart, D. E., & Klein, K. G. (2021). PATCH: Particle Arrival Time Correlation for Heliophysics. *Journal of Geophysical Research: Space Physics*, 126, e2020JA028940. <https://doi.org/10.1029/2020JA028940>

Received 14 NOV 2020
 Accepted 25 MAR 2021

PATCH: Particle Arrival Time Correlation for Heliophysics

J. L. Verniero¹ , G. G. Howes² , D. E. Stewart³ , and K. G. Klein⁴ 

¹Space Sciences Laboratory, University of California, Berkeley, Berkeley, CA, USA, ²Department of Physics and Astronomy, University of Iowa, Iowa City, IA, USA, ³Department of Mathematics, University of Iowa, Iowa City, IA, USA, ⁴Lunar and Planetary Laboratory, University of Arizona, Tucson, AZ, USA

Abstract The ability to understand the fundamental nature of the physics that governs the heliosphere requires spacecraft instrumentation to measure energy transfer at kinetic scales. This translates to a time cadence resolving the proton kinetic timescales, typically of the order of the proton gyrofrequency. The downlinked survey-mode data from modern spacecraft are often much lower resolution than this criterion, meaning that the higher resolution, burst-mode data must be captured to study an event at kinetic time scales. Telemetry restrictions, however, prohibit a sizable fraction of this burst-mode data from being downlinked to the ground. The field-particle correlation (FPC) technique can quantify kinetic-scale energy transfer between electromagnetic fields and charged particles and identify the mechanisms responsible for mediating the transfer. In this study, we adapt the FPC technique for calculating wave-particle energy transfer onboard modern spacecraft using time-tagged particle counts simultaneous with electromagnetic field measurements. The newly developed procedure, called Particle Arrival Time Correlation for Heliophysics (PATCH), is tested using synthetic spacecraft data, where output from a gyrokinetic plasma turbulence simulation was downsampled to Parker Solar Probe (PSP) energy-angle resolution. We assess the ability of the PATCH algorithm to recover the qualitative and quantitative features of the resulting velocity-space signatures, such as ion-Landau damping, that can be used to distinguish different kinetic mechanisms of particle energization. Ultimately, we demonstrate a proof-of-concept that the PATCH method could enable calculations of onboard wave-particle correlations, with the intent of enhancing spacecraft data return by several orders of magnitude.

1. Introduction

One of the greatest conundrums we have in modern spacecraft missions is the fact that instruments are capable of nearly continuously sampling high resolution, but due to telemetry limitations between the spacecraft and the Earth, we can afford to downlink only a small fraction of it. If we know *a priori* what kind of measurements we seek, data compression can be done by performing data analysis onboard the spacecraft and then sending back the post-processed data. That way, we would be able to gain insight from a larger fraction of the high-resolution data collected, and not limit our scientific return to a relatively small sample. In this study, we present a prescription for processing onboard measurements of turbulence-driven energy transfer from fields to particles.

Completely interpreting the turbulent cascade of energy, initially driven at large spatial scales (by phenomena such as solar granules or Coronal Mass Ejections) and dissipated at smaller scales into plasma heat (or some other form of particle energization), is the spearhead problem in space plasma turbulence. Understanding the nature of turbulent dissipation mechanisms that govern the physics in the transition region, from the inertial to the dissipation range of the turbulent spectrum of energy, is a key component in this puzzle. The field-particle correlation (FPC) technique can differentiate between mechanisms through its velocity-space signature; this is done by quantifying the energy transfer between fields and particles, as a function of velocity, after performing a long-time average of the Lorentz force term in the Vlasov equation (Chen et al., 2019; Howes et al., 2017; Klein & Howes, 2016; Klein et al., 2017). This study describes how we can adapt this method to develop an onboard wave-particle correlator using a new algorithm called Particle Arrival Time Correlation for Heliophysics (PATCH), enabling calculation of FPCs using discrete particle times of arrival and simultaneous field measurements. The SWEAP (Kasper et al., 2016) and FIELDS (Bale et al., 2016) instrument suites on the recently launched *Parker Solar Probe* (PSP) (Fox et al., 2016) is a prime

example of modern spacecraft instrumentation that would remarkably benefit from performing FPC calculations in real time, utilizing full burst-mode data resolution capabilities.

Resonant turbulent dissipation mechanisms, such as Landau damping and ion-cyclotron damping, are a natural initial focus for onboard wave-particle correlator methodology, toward applicable instrumentation. The FPC velocity-space signature of ion Landau damping is already well-understood (Howes et al., 2017; Klein et al., 2017; Klein & Howes, 2016), indicated by a change of the sign of the energy transfer between fields and particles from negative to positive about the resonant phase velocity of the kinetic Alfvén wave leading to a net transfer of energy to the particles and damping the wave. Therefore, this study will be dedicated to applying the PATCH algorithm to ion Landau damping. However, the method is general enough to differentiate between other proposed turbulent dissipation mechanisms, such as intermittent dissipation concentrated in current sheets and magnetic reconnection locations (Dmitruk et al., 2004; Karimabadi et al., 2013; Matthaeus & Montgomery, 1980; Osman, Kiyani, et al., 2014; Osman, Matthaeus, et al., 2014; Zhdankin et al., 2013, 2014) and nonresonant mechanisms, such as stochastic heating (Chandran, 2010; Chandran et al., 2010; Chen et al., 2001; Johnson & Cheng, 2001; Vech et al., 2017) and magnetic pumping (Lichko & Egedal, 2020; Lichko et al., 2017). *PSP* samples data in the inner heliosphere at extraordinary rates that could discern these mechanisms at relatively exceptional resolution. Successful implementation of the PATCH method enabling onboard computation of energy transport will therefore drastically improve the quality of downlinked in situ measurements of turbulent dissipation signatures at kinetic scales.

In order to adapt the FPC technique for onboard implementation, we first determined the minimum velocity-space resolution required by a spacecraft instrument to resolve the kinetic signature of ion Landau damping in our previous companion paper (Verniero et al., 2021). In Section 1.1, we review the history of attempts to build an onboard wave-particle correlator. In Section 1.2, we summarize the theory behind the FPC technique that distinguishes velocity-space signatures of particle acceleration mechanisms resulting from wave-particle interactions, such as Landau damping. We then apply this theory in Section 2 to construct the new PATCH algorithm, enabling onboard calculations of the field-particle energy transfer by utilizing the discrete particle times of arrival and the field measurements at the same times. In Appendix A, we employ a more formal derivation using kinetic theory. We discuss the implementation of PATCH in Section 3 using synthetic spacecraft data created by the Astrophysical Gyrokinetics code, AstroGK. The procedure is described in Section 3.1, producing results in Section 3.2 to qualitatively and quantitatively assess the performance of PATCH for resolving the velocity-space signature of Landau damping, which correspond to a specified sampling time for the instrument. A plan for analyzing downlinked *PSP* data for refinement of the PATCH method and eventual development of an onboard wave-particle correlator mission is discussed in Section 4, with conclusions following in Section 5.

1.1. History of Wave-Particle Correlators

Observations of wave-particle interactions have been sought over four decades. The earliest experiments flew on sounding rockets launched from Poker Flat, Alaska into the aurora, due to early speculation that resonant electrons preferentially “bunch” at a specific phase driven by large-amplitude Langmuir waves (Gough, Burke, et al., 1998; Gough, Hardy, et al., 1998; Gough & Urban, 1983; Gough et al., 1995, 1997, 1990; Rubin et al., 1999; Spiger et al., 1974, 1976; Lin et al., 1995; Woolliscroft et al., 1997). However, these were examples of particle auto-correlators that yielded information about the particle count rate statistics and not necessarily about energy transfer. The first true wave-particle correlator was constructed by Ergun et al. (1991), who correlated the phase of the waves with the electron time of arrival. Later, Kletzing et al. (2005) devised the University of Iowa wave-particle correlator, which acquired a phase bunching map by sorting electron counts into different phase bins. The wave-particle correlators developed by Ergun et al. (1991) and Kletzing et al. (2005), however, locked onto one dominant wave signal, yielding information about the relative phase of the electrons with respect to that wave. This type of procedure is not feasible in turbulence since there is a broadband spectrum of waves, with none being truly dominant.

A recent attempt to directly observe wave-particle interactions onboard spacecraft has been with the Wave-Particle Interaction Analyzer (WPIA) developed by Fukuhara et al. (2009). Their concept was implemented on the Arase mission (Katoh et al., 2013) and used on a ground-based analysis of *MMS* observations to diagnose a wave-particle event in the Earth's magnetosphere (Kitamura et al., 2018). Their method

computes the phase difference between the particles and waves by calculating the inner product between the electric field and the velocity of the plasma particles. The PATCH method differs from the WPIA by its unique ability to resolve the energy transfer as a function of velocity space, so the WPIA cannot be used in the same way as PATCH to distinguish different energization mechanisms in the heliosphere.

The early aforementioned correlators were designed to study electrons accelerated by Langmuir waves in the magnetosphere, but their results did not reveal useful information about the energy transfer dynamics in the aurora. Furthermore, the frequency of the Langmuir waves was at or above the counting rate on the particle detector. Solar wind turbulence, however, is dominated by Alfvénic fluctuations (Belcher & Davis, 1971; Bruno & Carbone, 2013; Howes & Nielson, 2013; Kraichnan, 1965; Verniero et al., 2018; Verniero & Howes, 2018; Verscharen et al., 2019) having much lower frequencies than Langmuir waves. The modern spacecraft instruments on PSP are capable of particle count rates greater than these wave frequencies, enabling new strategies for detecting wave-particle interactions of interest to the turbulence community. The primary goal of this study is to understand energization of particles due to the damping of turbulent fluctuations.

1.2. The FPC Technique

The FPC technique quantifies the net energy transfer between the electromagnetic fields and the plasma particles as a function of particle velocity, producing a distinct *velocity-space signature* for diagnosing and distinguishing turbulent dissipation mechanisms (Howes et al., 2017; Klein & Howes, 2016; Klein et al., 2017). The first direct evidence of electron Landau damping in a turbulent space plasma was recently illuminated using *Magnetospheric Multiscale Mission (MMS)* magnetosheath observations by Chen et al. (2019). Implementing the FPC technique onboard spacecraft is therefore a natural extension of this method. As a starting point for the discussion of how to modify the method for onboard use, we briefly summarize the derivation of the standard, ground-based FPC method below.

On the short time scale of the energization of particles by turbulence in a weakly collisional plasma, the evolution of the six-dimensional (3D-3V) velocity distribution function $f_s(\mathbf{r}, \mathbf{v}, t)$ for each species s is given by the Vlasov equation,

$$\frac{\partial f_s}{\partial t} + \mathbf{v} \cdot \nabla f_s + \frac{q_s}{m_s} \left[\mathbf{E} + \frac{\mathbf{v} \times \mathbf{B}}{c} \right] \cdot \frac{\partial f_s}{\partial \mathbf{v}} = 0, \quad (1)$$

and the system is closed with Maxwell's equations. Here, c is the speed of light, \mathbf{v} is the particle velocity, \mathbf{E} is the electric field, and \mathbf{B} is the magnetic field. The third term, the Lorentz force term, governs the interactions between the fields and particles.

Summarizing the derivation by Howes et al. (2017), multiplying Equation 1 by $m_s v^2$ yields an equation for the instantaneous rate of change of *phase-space energy density*, $w_s(\mathbf{r}, \mathbf{v}, t) = \frac{1}{2} m_s v^2 f_s(\mathbf{r}, \mathbf{v}, t)$, given by

$$\frac{\partial w_s(\mathbf{r}, \mathbf{v}, t)}{\partial t} = -\mathbf{v} \cdot \nabla w_s - q_s \frac{v^2}{2} \mathbf{E} \cdot \frac{\partial f_s}{\partial \mathbf{v}} - q_s \frac{v^2}{2} \left(\frac{\mathbf{v} \times \mathbf{B}}{c} \right) \cdot \frac{\partial f_s}{\partial \mathbf{v}}. \quad (2)$$

When Equation 2 is integrated over all velocity and physical space with appropriate boundary conditions (periodic or boundaries at infinity), only the electric field term (second term on the right-hand side) is nonzero. However, missions with one (or only a few) spacecraft do not provide the information needed for the spatial integration. Instead, we employ the observationally accessible 3V information measured at a single-point, $\mathbf{r}_0 = (x_0, y_0, z_0)$, to determine the rate of change of energy density at \mathbf{r}_0 . The electric field term describes both the physics of the secular energy transfer that leads to net particle energization and the physics of the oscillating energy transfer associated with undamped wave motions. Therefore, a time-average over a sufficiently long *correlation interval* τ is taken to eliminate the oscillating signal, yielding the *standard FPC*, $C_E(\mathbf{r}_0, \mathbf{v}, t, \tau)$, defined by

$$C_E(\mathbf{r}_0, \mathbf{v}, t, \tau) = \frac{1}{\tau} \int_{t-\tau/2}^{t+\tau/2} dt' \left[-q_s \frac{v^2}{2} \frac{\partial f_s(\mathbf{r}_0, \mathbf{v}, t')}{\partial \mathbf{v}} \cdot \mathbf{E}(\mathbf{r}_0, t') \right] \quad (3)$$

Note that the v^2 term in Equation 3 is substituted with v_i^2 for $i \in \{v_{\parallel}, v_{\perp 1}, v_{\perp 2}\}$ depending on which component of $\mathbf{E} = \{E_{\parallel}, E_{\perp 1}, E_{\perp 2}\}$ is being correlated with f_s . For example, in the case of Landau damping, we are interested in the parallel contributions of the electric field E_{\parallel} with the particle velocities v_{\parallel} , so the dot product in Equation 3 converts to multiplication. The standard FPC, $C_E(\mathbf{r}_0, \mathbf{v}, t, \tau)$, generates a *velocity-space signature* of energy transfer in 3V velocity space that is characteristic of the mechanism of energization. Integration over velocity-space yields the time-averaged net rate of change of spatial energy density of species s due to the electric field, $\int d^3\mathbf{v} C_E(\mathbf{r}_0, \mathbf{v}, t, \tau) = \langle \mathbf{j}_s \cdot \mathbf{E} \rangle_{\tau}$, where $\langle \rangle_{\tau}$ indicates a time-average over τ .

The velocity derivative in the standard FPC given by Equation 3 prevents a straightforward implementation of this method onboard a spacecraft. Instead, we use an alternative version of the FPC derived by substituting $f_s = 2w_s/mv^2$ into Equation 1 and manipulating the equations into the form

$$\frac{dw_s}{dt} = \frac{\partial w_s(\mathbf{r}, \mathbf{v}, t)}{\partial t} + \mathbf{v} \cdot \nabla w_s + \frac{q_s}{m_s} \left[\mathbf{E} \cdot + \frac{\mathbf{v} \times \mathbf{B}}{c} \right] \cdot \frac{\partial w_s}{\partial \mathbf{v}} = q_s \mathbf{v} \cdot \mathbf{E} f_s \quad (4)$$

This equation can be interpreted as the rate of change of phase-space energy density $w_s(\mathbf{r}, \mathbf{v}, t)$ along Lagrangian particle trajectories in 3D-3V phase space (where d/dt represents the Lagrangian derivative in 3D-3V). The right-hand side of Equation 4 thus shows that the rate of change along particle orbits is solely due to the rate of work done on the particles by the electric field. From this perspective, the standard form in Equation 2 represents an Eulerian formulation for the rate of change of phase-space energy density $w_s(\mathbf{r}, \mathbf{v}, t)$ at a fixed point in 3D-3V phase space. Therefore, we define the alternative FPC, $C'_E(\mathbf{r}_0, \mathbf{v}, t)$, by

$$C'_E(\mathbf{r}_0, \mathbf{v}, t, \tau) \equiv \frac{1}{\tau} \int_{t-\tau/2}^{t+\tau/2} dt' q_s f_s(\mathbf{r}_0, \mathbf{v}, t') \mathbf{v} \cdot \mathbf{E}(\mathbf{r}_0, t') \quad (5)$$

Note that when integrated over all velocity space, both correlations defined by Equations 3 and 5 yield the same result: the time-averaged rate of work done by the electric field on the particle species s , $\langle \mathbf{j}_s \cdot \mathbf{E} \rangle_{\tau}$. The integrand of Equation 5 is the general form upon which the PATCH onboard implementation of the FPC technique is based, where parallel or perpendicular components of \mathbf{E} can be separated to explore different energization mechanisms, given by $C'_{E_{\parallel}}$ or $C'_{E_{\perp}}$.

2. Onboard Spacecraft Measurements

Instruments onboard spacecraft can sample the plasma at their maximum high-resolution cadence, but due to telemetry restrictions, only a small fraction of the highest resolution data can be transmitted to the ground for analysis. Onboard correlation calculations enables an efficient use of the highest resolution measurements of an instrument, maximizing scientific data return by only downlinking time-averaged energy transfer information as a form of data compression. This section serves as proof-of-concept that the proposed, prototypical methodology could indeed achieve this goal. We develop a simple way to perform FPC calculations onboard spacecraft, called the Particle Arrival Time Correlation for Heliophysics (PATCH) algorithm. We demonstrate a simplified derivation in Section 2.2 and show it is consistent with more rigorous kinetic theory developed in Appendix A.

2.1. Particle Arrival Time

Before deriving the PATCH method for FPC implementation onboard spacecraft, we first define a *particle arrival time*. As discussed in Section 2.2, the PATCH algorithm is based on time-tagging particle counts; the definition of the “time” a particle is “counted” on a spacecraft must be clearly defined to link the theory behind PATCH to physical observations and make improvements based on instrumental specifications.

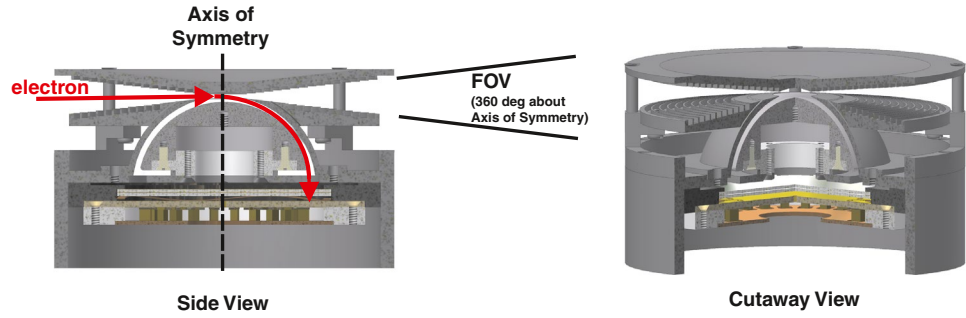


Figure 1. Physical picture of “top-hat” ESA design, including a side view (left) of the electron particle trajectory (red) crossing the symmetry axis (dotted black line). The field-of-view (FOV) spins 360° around this axis, which also defines the area of the aperture opening. The cutaway view (right) shows the two nested hemispheres responsible for the net voltage difference.

This section describes background material about spacecraft particle detectors, facilitating a more precise definition of a particle arrival time.

The particle detector on a spacecraft is generally of a type known as an Electrostatic Analyzer (ESA), with typical modern configurations as a “top-cap” design (Carlson et al., 1982), shown in Figure 1. Physically, it is a cylindrically symmetric configuration consisting of a particle entrance *aperture* on top of two nested hemispheres. The aperture entrance is a cylindrical figure of revolution, also known as the field-of-view (FOV), which rotates 360° about an axis of symmetry (see left side view in Figure 1). The axis of this rotation is symmetric about the set voltage difference of the two nested hemispheres (see right cutaway view in Figure 1), which will select particles of species s , and charge q_s , with energy E .

The particle arrival time is defined as the time, t_p , that the particle crosses the surface area of the entrance aperture in Figure 1; this is a curvilinear surface approximated locally as a 2D rectangle with an infinitesimal slab of area, \mathbf{A} , in a plane parallel to the azimuthal axis of symmetry. The ESA then collects these particles, which arrive at an angle of incidence, approximately normal to the surface of the aperture plane, with a specific time, position, and velocity. This information at the particle arrival time, t_p , is then recorded into five measurement bins encompassing six-dimensional phase-space: (1) 1D azimuthal angle ϕ , (2) 1D polar angle θ , (3) 1D energy E , (4) 1D velocity v , and (5) 2D position area \mathbf{A} . The width of these bins, Δ , determines the data resolution; a smaller Δ enables a finer measurement grid to yield better resolution, and vice versa.

The finiteness of physical hardware invokes a natural upper bound on the instrumental resolution quality. The geometric factor, also referred to as the \mathcal{G} -factor, is defined as

$$\mathcal{G} = \frac{\Delta E}{E} \Delta \mathbf{A} \Delta \Omega \quad (6)$$

where $\Delta E/E$ is the energy response (equal to a constant) and Ω is the solid angle of rotation, combining ϕ and θ . In addition, any prediction made from kinetic plasma theory must account for breaking the assumption that measurements are sampled continuously. The PATCH algorithm specifically utilizes the discreteness of particle count measurements to optimize accuracy of calculating quantities existing in the physical universe.

2.2. Demonstration of the PATCH Algorithm

On a spacecraft, the standard phase-space (\mathbf{r}, \mathbf{v}) distribution function, f_s , is defined as,

$$f_s = \frac{N}{d^3 \mathbf{r} d^3 \mathbf{v}} \quad (7)$$

where N is the number of species s particles, with mass m , counted in some infinitesimal region of phase-space, $d^3 \mathbf{r} d^3 \mathbf{v}$. In reality, the detector counts particles with discrete arrival times, defined as the time the

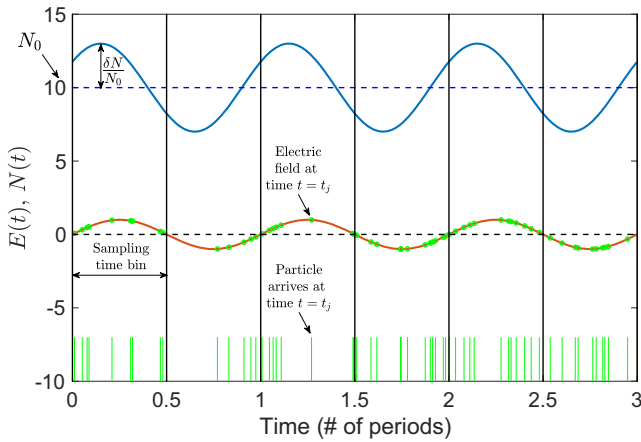


Figure 2. 2D representation of the PATCH procedure in a single 6D phase-space bin ($\Delta \mathbf{r}_p, \Delta \mathbf{v}_p$). The blue curve, $N(t)$, represents the number density of particles in this bin. The green vertical lines indicate particles arriving with probabilities dictated by $N(t)$. The red curve is the electric field, $E(t)$, with open green circles, indicating that the electric field is evaluated at the particle time of arrival. The summation of these values with appropriate normalization yields the correlation, C_τ^* , in this bin.

particle enters the aperture, described in Section 2.1. Thus, the observed number of particles in the single phase-space bin $\Delta \mathbf{r}_p \Delta \mathbf{v}_p$ is given by

$$N_{obs}(t) = \sum_{j=1}^{N_{tot}} \delta(t - t_j) \quad (8)$$

over a sampling time dt . The total number of particles counted, centered at time t_p over the appropriate correlation time, τ , is

$$N_\tau = \int_{t_p - \frac{\tau}{2}}^{t_p + \frac{\tau}{2}} dt N_{obs}(t) \quad (9)$$

which is interpreted as the count rate over the correlation time interval, τ .

Based on the observed distribution function defined by Equation 7, we now define a specific physical distribution function observed by the spacecraft particle detector with an aperture geometry-defined phase-space to intuitively derive the PATCH method. In a single phase-space bin, there is a fixed point in space \mathbf{r}_p and velocity \mathbf{v}_p

$$f_s(\mathbf{r}_p, \mathbf{v}_p, t) = \frac{N_{obs}(t)}{\Delta \mathbf{r}_p \Delta \mathbf{v}_p} \quad (10)$$

where $N_{obs}(t)$ is the number of particle counts observed as a function of time given by Equation 8. By substituting Equation 10 into the RHS of Equation 4, the rate of change of phase-space energy density due to the electric field is approximated as

$$\left(\frac{dw(\mathbf{r}_p, \mathbf{v}_p, t)}{dt} \right)_{\mathbf{E}} \approx q_s \mathbf{v}_p \frac{N_{obs}(t) \mathbf{E}(\mathbf{r}_p, t)}{\Delta \mathbf{r}_p \Delta \mathbf{v}_p} \quad (11)$$

Equation 5 says that the correlation over some time, τ , determines the rate of change of particle energization:

$$C_\tau^* \langle q_s N_{obs}(t) \mathbf{v}_p \cdot \mathbf{E}(t) \rangle = \frac{1}{\tau} \int_{t-\tau/2}^{t+\tau/2} dt' q_s N_{obs}(t') \mathbf{v}_p \cdot \mathbf{E}(t') \quad (12)$$

The correlation, C_τ^* , constructed from discrete particle arrival times (in a single phase-space bin) is then

$$C_\tau^* = \frac{1}{\tau} \sum_{j=1}^{N_\tau} \int dt \delta(t - t_j) q_s \mathbf{v}_p \cdot \mathbf{E}(t) = \frac{1}{\tau} \sum_{j=1}^{N_\tau} q_s \mathbf{v}_p \cdot \mathbf{E}(t_j) \quad (13)$$

The PATCH algorithm, based on Equation 13, is simply the summation of the electric field evaluated at the particle arrival times over the correlation interval, τ . Because the electric field is not summed uniformly over time, but only at the particle arrival times, it captures the critical phase relationship between the electric field and the fluctuations in the particle velocity distribution, which determines the net collisionless transfer of energy between the fields and particles. Note that Appendix A presents a formal derivation of the PATCH methodology (Equation A25) starting from kinetic theory.

As a simple demonstration shown in Figure 2, consider a sinusoidal electric field (red) with a known time evolution at the point of measurement \mathbf{r}_p and sinusoidal particle number density $N(t)$ (blue) within a single ($\Delta \mathbf{r}_p, \Delta \mathbf{v}_p$) phase-space bin. In this simple 1D example represented by Figure 2, $e(t)$ represents the 1D component of the electric field we are interested in correlating with $N(t)$. In the case of Landau damping, which is mediated by the parallel component of the electric field, this component would be E_{\parallel} . The particles arrive (green vertical lines) in a Poisson-distributed manner with probabilities dictated by $N(t)$, which can be interpreted as the number of particle counts within a sampling time, dt_p , that enter the aperture as a function

of time. Hence, $N(t)$ is simply the count rate in each phase-space bin. The in-phase component between $N(t)$ and $E(t)$ is what leads to net energy transfer, since only the in-phase components contribute to a non-zero value of the integral in Equation 12 over an integer number of periods.

To find the correlation over the interval, $\tau = 3$ periods, we perform the following procedure. If a particle arrives at some time, $t = t_j$, represented by the green vertical lines in Figure 2, then the electric field is evaluated at that time, $E(t_j)$, represented by the green circles. We then multiply $E(t_j)$ by the velocity, v_p , and compute the summation given by Equation 13 over a sufficiently long time interval, τ .

3. Testing PATCH With Synthetic Spacecraft Data

We now present a demonstration of the PATCH algorithm, using it to diagnose ion Landau damping in a gyrokinetic plasma turbulence simulation utilizing the Astrophysical Gyrokinetics code AstroGK (Numata et al., 2010). We describe the procedure for implementing PATCH with the simulation output data in Section 3.1, along with results demonstrating that the ion Landau damping velocity-space signature can be resolved with this novel method in Section 3.2.

3.1. PATCH Implementation Procedure

The PATCH algorithm can be tested using a time series of the electromagnetic fields and ion velocity distributions at a single spatial point in a driven AstroGK simulation of strong plasma turbulence for a $\beta_i = 1$ and $T_i/T_e = 1$ plasma, detailed in Klein et al. (2017). The 3D-2V gyrokinetic simulation employs a resolution of $(n_x, n_y, n_z, n_\lambda, n_E, n_s) = (64, 64, 32, 64, 32, 2)$, where n_λ is the number of pitch angles, n_E is the number of energies, and n_s is the number of species (protons or electrons). The fully resolved spatial dynamic range of the simulation spans $0.25 \leq k_\perp \rho_i \leq 5.5$, and 2V velocity-space is resolved by $n_E \times n_\lambda = 32 \times 64 = 2,048$ grid points. In addition, a reduced mass ratio of $m_p/m_e = 32$ is employed.

Our companion paper (Verniero et al., 2021) describes a procedure for constructing synthetic spacecraft data downsampled to the PSP spacecraft energy-angle resolution. The ion electrostatic analyzer instrument, SPAN-I in the PSP SWEAP particle instrument suite (Kasper et al., 2016), boasts maximum energy and azimuthal angle phase-space resolution $\frac{\Delta E}{E} \times \Delta \phi = 7\% \times 3.75^\circ$. This synthetic data procedure uses output of the 2V gyrokinetic perturbed ion distribution function $g_i(v_\parallel, v_\perp, t)$ from a single spatial point in the simulation domain, at a uniform time interval Δt , as well as the value of the electric field at the same position and times. This time series of g_i at times t_i is combined with a constant Maxwellian equilibrium $F_{0i}(v)$, with ion temperature $T_i = 8.6$ eV, to generate a total 2V ion distribution function,

$$f_i(v_\parallel, v_\perp, t_i) = F_{0i}(v) + \epsilon g_i(v_\parallel, v_\perp, t_i) \quad (14)$$

Here, $\epsilon \sim \delta f_i/F_{0i} = 0.1$ is the gyrokinetic expansion parameter that specifies the amplitude of the perturbed ion distribution function relative to the equilibrium. This ion distribution function in the plasma rest frame is then boosted to the solar wind velocity (relative to the spacecraft), chosen here to be $v_{sw} = 400$ km/s with an angle between the solar wind flow and the magnetic field of $\alpha = 30^\circ$. The resulting spacecraft-frame ion velocity distribution function is then downsampled to the instrumental resolution in energy-azimuthal angle coordinates (E, ϕ) and scaled by the peak of the Maxwellian equilibrium. This procedure yields a normalized total ion velocity distribution function

$$\hat{f}_i(E_j, \phi_k, t_l) = \frac{f_i(E_j, \phi_k, t_l)}{F_{0i}(v=0)} \quad (15)$$

for energy bin E_j and azimuthal angle bin ϕ_k , at time t_l .

To implement a test for the PATCH algorithm using the downsampled synthetic ion velocity distribution function f_i from the procedure outlined in Verniero et al. (2021), we detail here a final step, utilizing f_i to generate a time series of particle counts at the detector aperture in each of the energy-angle phase space bins

(E_j, ϕ_k) . This is accomplished by using the normalized \hat{f}_i in each (E_j, ϕ_k) bin to determine the probability of counting particles in that bin. Note that the maximum value of the normalized ion distribution function is ~ 1 , i.e., $\max(\hat{f}_i) \approx 1$. Given that $\hat{f}_i(E_j, \phi_k) = 1$, we define N as the average number of particles counted in a single (E_j, ϕ_k) bin. Since the value of the ion distribution function decreases rapidly away from the center of the velocity distribution, most (E_j, ϕ_k) bins will have far fewer than N counts during one sampling interval. This definition of N enables us to characterize the number of particle counts needed in each (E_j, ϕ_k) bin to resolve a meaningful velocity-space signature using the PATCH algorithm.

To create the time series of counts in each (E_j, ϕ_k) bin with the appropriate Poisson statistics, we adopt the following procedure. For a specified maximum value of N counts per bin, we divide the sampling interval Δt into N equal sub-intervals. In each sub-interval, we use the value of $\hat{f}_i(E_j, \phi_k)$ as the probability that a single particle is counted in that sub-interval. If a particle is counted, the parallel electric field (since we are seeking the signature of ion Landau damping), output from the AstroGK simulation at the sampling interval cadence Δt , is linearly interpolated to the sub-interval time t_n ; this denotes the *particle arrival time*, yielding $E_{\parallel}(t_n)$. The resulting set of particle arrival times t_n , governed by Poisson statistics, is analogous to the green vertical lines in Figure 2; and the nonuniform series of $E_{\parallel}(t_n)$ measurements at each of these arrival times corresponds to the green circles on the red electric field curve. Thus, the parallel electric field measurements are weighted by the particle counts.

For a given sampling interval l and phase-space bin (E_j, ϕ_k) , we denote the total number of particles counted by N_{jkl} . For each (E_j, ϕ_k) bin, we also compute the corresponding velocities parallel and perpendicular to the magnetic field *in the frame of the time-averaged ion bulk flow*, denoted $v_{\parallel jk}$ and $v_{\perp jk}$, respectively. For a correlation interval τ consisting of L sampling intervals, such that $\tau = L\Delta t$, we use Equation 13 to obtain the PATCH correlation $C_{E_{\parallel}}^*$. The rate of work done by the parallel electric field is thus given by,

$$C_{E_{\parallel}}^*(v_{\parallel jk}, v_{\perp jk}, t, \tau) = \frac{1}{\tau} \sum_{l=1}^L \frac{1}{\Delta \mathbf{r}_p \Delta \mathbf{v}_p} \sum_{n=1}^{N_{jkl}} q_i v_{\parallel jkl} E_{\parallel}(t_{nl}) \quad (16)$$

where the time indicated for the correlation t is at the center of the correlation interval τ . This equation matches Equation A25 from the formal derivation detailed in Appendix A.

3.2. Performance of the PATCH Algorithm

In analyzing particle energization in heliospheric plasmas, the PATCH algorithm aims to achieve the same two goals as the ground-based FPC technique: (i) to generate a *velocity-space signature* that can be used to distinguish the different kinetic mechanisms governing the energy transfer; and (ii) to yield a quantitative estimate for the rate of change of spatial energy density by an integration of the PATCH correlation over velocity-space. In this section, we assess the ability of the PATCH algorithm to achieve both of these goals as the characteristic number of particle counts per energy-angle bin, N , is varied.

Recall that the characteristic single-bin particle count N is defined as the average number of particles that would be counted in a single energy-angle bin (E_j, ϕ_k) , given that the normalized distribution function for that bin is $\hat{f}_i(E_j, \phi_k) = 1$. Physically, the value of N is a measure of the particle count rate by the instrument; and therefore, it depends on the local plasma number density n_0 , the sampling time for the single bin Δt , and the geometric \mathcal{G} -factor of the instrument, given by Equation 6. This description of N directly corresponds to the mean number density, N_0 , of the simplified single-bin model shown in Figure 2.

Note that the rate of energy transfer given by Equation 16 will statistically be linearly proportional to N . Since the summand of Equation 16 is the rate of work done on an ion with charge q_i and parallel velocity v_{\parallel} by the parallel component of the electric field E_{\parallel} , it is physically reasonable that a larger number of ions counted will correspond to a larger energy transfer rate. Therefore, to assess the ability of the PATCH method to recover the qualitative features of the velocity-space signature and the quantitative value of the velocity-integrated energy transfer rate, the correlation given by Equation 16 may be scaled by $1/N$ to enable a quantitative comparison between PATCH results with varying N values. Any differences will be caused by

the Poisson statistics of the particle counts in each bin, enabling us to assess the performance of the PATCH algorithm as N is varied.

3.2.1. Qualitative Test

Here, we test the ability of the algorithm to qualitatively reproduce the known velocity-space signature of ion Landau damping, which has previously been recovered from a strong turbulence simulation of a $\beta_i = 1$ and $T_i/T_e = 1$ plasma using the FPC technique (Klein et al., 2017). As explained in Section 1.2, the velocity derivative in Equation 3 poses difficulties for implementation of the FPC concept when only supplied with individual particle counts. For the PATCH method, we thus begin with the alternative form of the correlation given by Equation 5. The velocity-space signature of the alternative correlation, $C'_{E_{\parallel}}(v_{\parallel}, v_{\perp}, t)$, for ion Landau damping qualitatively shows that the peak of the rate of energy transfer occurs at the parallel resonant velocity, $v_{\parallel}/v_{ti} \simeq 1$ and is accompanied with a zero-crossing that shifts to lower parallel velocities $v_{\parallel}/v_{ti} < 1$. This feature has a smaller amplitude minimum, as shown in the timestack plot of $C'_{E_{\parallel}}(v_{\parallel}, t)$ in Figure 9c of Klein et al. (2017). Ultimately, using the PATCH algorithm, we seek to reproduce these qualitative and quantitative features of the velocity-space signature of ion Landau damping from the alternative correlation $C'_{E_{\parallel}}(v_{\parallel}, v_{\perp}, t)$.

In Figure 3, we plot the parallel PATCH correlation in gyrotropic velocity space $C^*_{E_{\parallel}}(v_{\parallel}, v_{\perp}, t, \tau)$ given by Equation 16 for a correlation interval $\tau\omega_A = 10.4$ (where the domain-scale Alfvén waves driving the turbulence have periods $T\omega_A = 2\pi$). We compare the qualitative pattern of the velocity-space signature of the energy transfer using the PATCH method, $C^*_{E_{\parallel}}$, for varying single-bin particle counts N in panels (a–g), to the velocity-space signature from the alternative FPC $C'_{E_{\parallel}}$ in panel (h). In these plots, the black dots indicate the bin centers of the energy-azimuthal angle bins (E, ϕ) using realistic instrumental resolution for the PSP spacecraft. At this resolution, the velocity-space range over $-4 \leq v_{\parallel}/v_{ti} \leq 4$ and $0 \leq v_{\perp}/v_{ti} \leq 4$ in the ion plasma rest frame is sampled by just 129 energy-angle bins (Verniero et al., 2021). The key qualitative features in the alternative FPC $C'_{E_{\parallel}}$ in Figure 3h that are indicative of ion Landau damping are: (i) the significant positive peak just above $v_{\parallel}/v_{ti} = 1$ at approximately the expected parallel resonant velocity, (ii) the zero crossing just below $v_{\parallel}/v_{ti} = 1$, and (iii) the smaller negative dip at smaller values of v_{\parallel} . This is the velocity-space signature that we aim to recover with the PATCH algorithm.

The comparison in Figure 3 demonstrates that the PATCH method $C^*_{E_{\parallel}}$ converges qualitatively to the alternative FPC $C'_{E_{\parallel}}$ as N increases, with most of the finer features of $C'_{E_{\parallel}}$ recovered for values $N \gtrsim 75$. Furthermore, although the quantitative amplitudes of the features are slightly altered by the variation inherent to the Poisson sampling statistics, the broader qualitative pattern of energization in velocity space is still reproduced reasonably well for values down to $N = 16$, recovering the features needed to identify ion Landau damping. For $N < 16$, the qualitative features of the velocity-space signature are lost, or at least distorted, by the random error. Therefore, it appears that in Figure 3b that for $N \gtrsim 16$, the PATCH algorithm indeed succeeds in recovering the characteristic signature of ion Landau damping found by the alternative FPC $C'_{E_{\parallel}}$ shown in Figure 3h, which is the correlation at PSP SPAN-I instrumental resolution without incorporating Poisson sampling statistics.

3.2.2. Quantitative Test

The second test is to quantitatively assess the accuracy of the rate of change of ion spatial energy density $dw_i(\mathbf{r}, t) / dt$ due to the parallel electric field, E_{\parallel} ; this is determined by the integration over velocity space of the parallel PATCH method, denoted $(dw_i(\mathbf{r}_0, t) / dt)_{E_{\parallel}} = \int d^3\mathbf{v} C^*_{E_{\parallel}}(v_{\parallel}, v_{\perp})$. We compare the resulting $(dw_i / dt)_{E_{\parallel}}$ from the PATCH method with varying N , to the “exact” result arising from the velocity-space integration of the alternative FPC $\int d^3\mathbf{v} C'_{E_{\parallel}}(v_{\parallel}, v_{\perp})$, as shown in Figure 3h. In Figure 4, we calculate the rate of change of ion spatial energy density as a function of time using the alternative FPC C' (exact, black), compared to the PATCH method $C^*_{E_{\parallel}}$ with $N = 16$ (magenta), 25 (cyan), 50 (blue), 100 (green), and 1000 (red). The results again show that the PATCH method $C^*_{E_{\parallel}}$ converges to the alternative FPC C' result as N

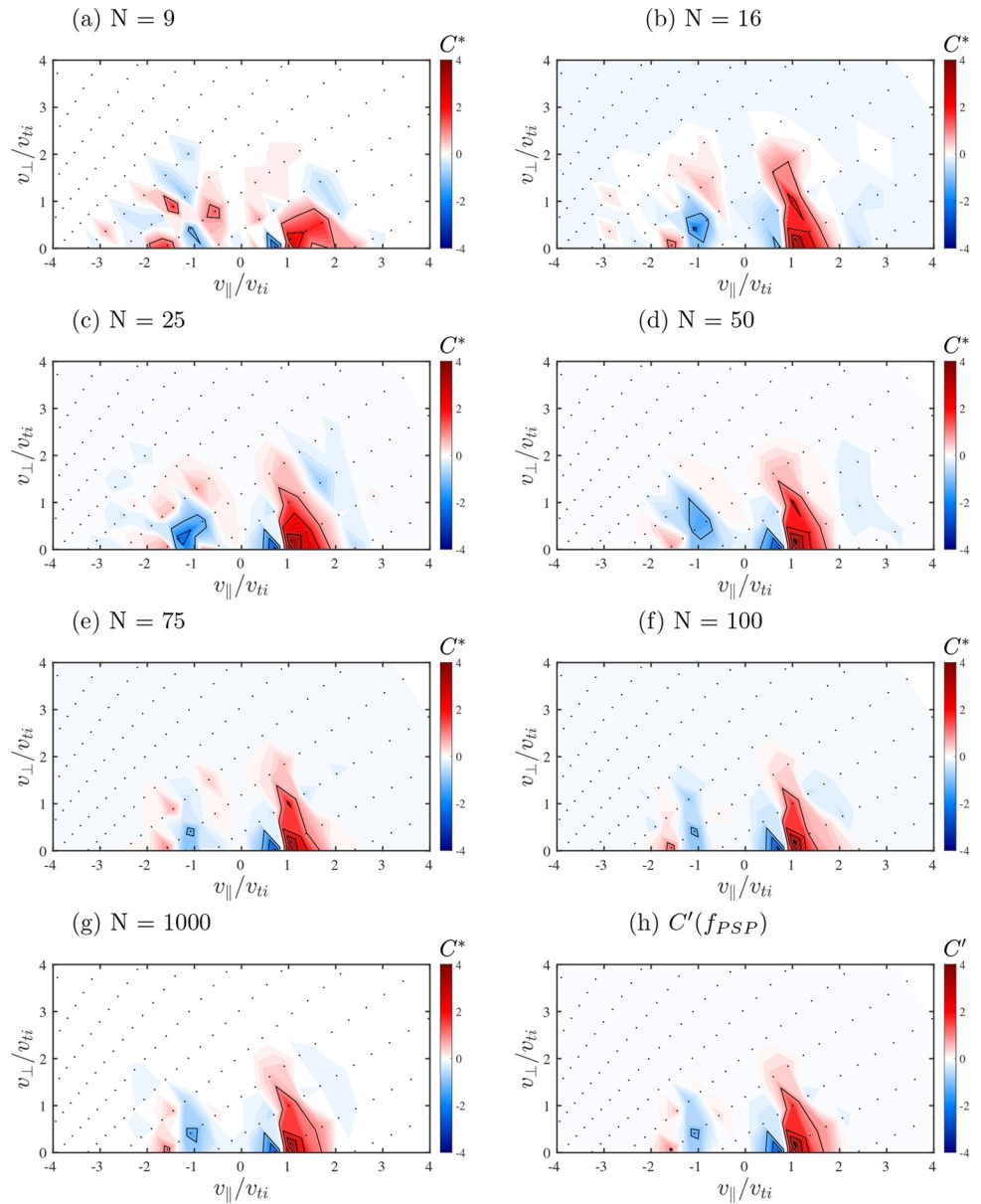


Figure 3. Testing the ability of the PATCH algorithm to recover the velocity-space signature of ion Landau damping, using the particle arrival time correlation, $C_{E_{\parallel}}^*$, in PSP resolution for single-bin particle counts (a) 9, (b) 16, (c) 25, (d) 50, (e) 75, (f) 100, and (g) 1,000 particles. Comparison to using the alternate FPC at PSP resolution, $C'(f_{PSP})$ (Verniero et al., 2021), instead of the PATCH method, is represented in panel (h).

increases. Furthermore, even at the lowest value of $N = 16$ (magenta), the PATCH algorithm still captures the broader trend of the ion energization as a function of time, with a loss of ion energy at $t\omega_A < 10$, and an increasing rate of ion energization later in the simulation.

To evaluate how the accuracy of the rate of change of ion spatial energy density $(dw_i(\mathbf{r}_0, t) / dt)_{E_{\parallel}}$ changes with N , at time $t\omega_A = 13.9$ in the simulation (vertical dot-dash line in Figure 4), we perform an ensemble of 16 independent realizations of the PATCH algorithm for each value of N . We verify that the mean value for $(dw_i(\mathbf{r}_0, t) / dt)_{E_{\parallel}}$ of these realizations converges to C_{PSP} as N increases. But, onboard a spacecraft, we are not able to make repeated measurements of the same plasma volume, and therefore cannot obtain an

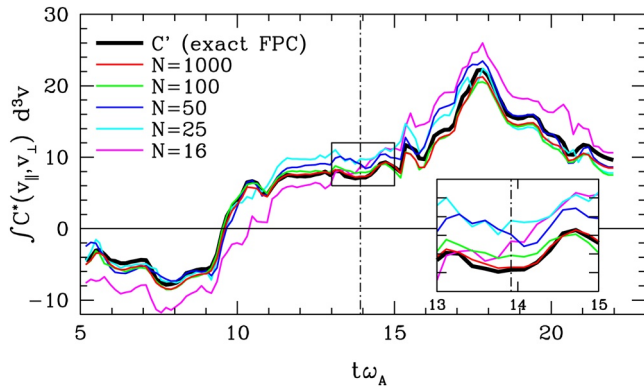


Figure 4. Comparison of the rate of ion energization computed by integration of the FPC $\int d^3v C^*(v_{\parallel}, v_{\perp})$ (black) to that computed by the integration of the PATCH $\int d^3v C^*(v_{\parallel}, v_{\perp})$ with $N = 1000$ (red), 100 (green), 50 (blue), 25 (cyan), and 16 (magenta). The vertical dash-dotted line indicates the time at which the correlations in Figure 3 were calculated.

accurate determination of the time-averaged energy transfer at a given point in space. The plasma is streaming past the spacecraft at typically supersonic and super-Alfvénic velocities, and so the accuracy of our answer is more practically assessed by observing the variation of the energy transfer rate among the 16 realizations at each value of N .

In Figure 5a we plot the average value of $(dw_i(\mathbf{r}_0, t) / dt)_{E_{\parallel}}$ (indicated by the blue asterisks) after performing these 16 realizations. The red horizontal dashed-dotted line at $(dw_i(\mathbf{r}_0, t) / dt)_{E_{\parallel}} = 7.1607$ represents C'_{PSP} ; we note that the error bars decrease as $N \rightarrow 1000$ and that $(dw_i(\mathbf{r}_0, t) / dt)_{E_{\parallel}} \rightarrow 7.1607$. In Figure 5b, we visualize this error as the percentage of the standard deviation $\sigma(N)$ relative to the “exact” value of $(dw_i(\mathbf{r}_0, t) / dt)_{E_{\parallel}}$ computed from C'_{PSP} ; this measure of the error also converges for sufficiently large N . Furthermore, for values of $N \gtrsim 100$, the random statistical error of the PATCH algorithm is $\approx 20\%$, which is the average error of the energy transfer rate determination found in Verniero et al. (2021) due to the limited instrumental phase-space resolution of the

PSP mission (relative to the much higher velocity-space resolution results of the AstroGK simulation). Existing methods for the determination of the particle energization rate in heliospheric plasma turbulence often yield at best order-of-magnitude estimates. Therefore, even at very low single-bin particle counts of $N \sim 25$, with its estimated error around 45%, the PATCH algorithm still represents a useful approach to measure the rate of energization of particles relative to state-of-the-art modern spacecraft instrumentation.

In summary, the demonstration of the PATCH algorithm presented here shows that (i) the PATCH algorithm recovers qualitatively accurate velocity-space signatures of particle energization for $N \gtrsim 16$ and quantitatively accurate velocity-space signatures for $N \gtrsim 75$; (ii) the time evolution of the rate of particle energization is well captured qualitatively for $N \gtrsim 16$ with an error that converges for $N \rightarrow 1000$; and (iii) the accuracy of the rate of particle energization for $N \gtrsim 100$ reaches the level of 20%, the same level limited by the instrument resolution for PSP (Verniero et al., 2021).

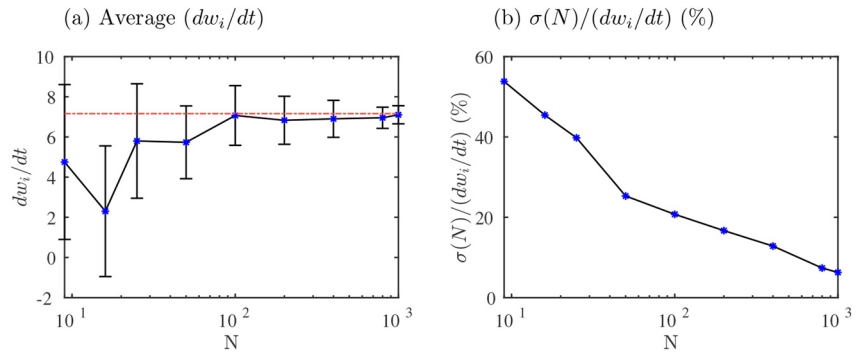


Figure 5. Demonstration of the PATCH error where (a) shows the average of the velocity-integrated energy transfer rate (dw_i/dt) for an ensemble of 16 PATCH realizations at each N marked by the blue asterisk, with the standard deviation as error bars. The red horizontal dashed line represents the “exact” value of $(dw_i(\mathbf{r}_0, t) / dt)_{E_{\parallel}}$ computed from the alternative FPC C' (using synthetic data downsampled to PSP instrumental resolution); and (b) represents the standard deviation of the error as a percentage of the transfer rate.

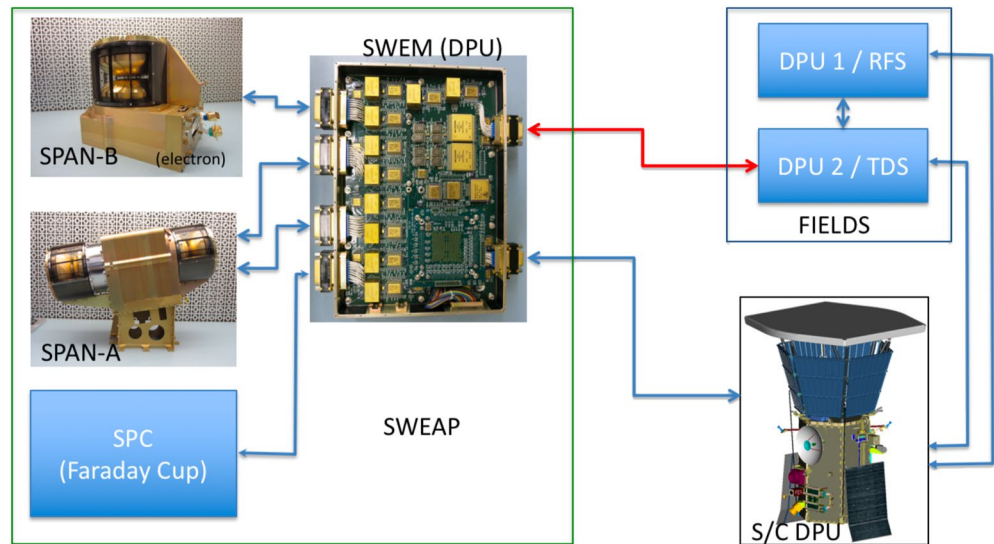


Figure 6. The SWEAP/FIELDS interface on PSP: the Wave-Particle Correlator (WPC).

4. Future In-Situ Testing

The PATCH method was conceived with the new capabilities of *PSP* in mind. It has been tested and analyzed with theoretical simulations, but future work will test and refine this method using actual spacecraft data. The initial perihelion datasets from *PSP* have shown strong evidence of wave-particle interactions and related kinetic instabilities (Bale et al., 2019; Bowen et al., 2020; Malaspina et al., 2020; Verniero et al., 2020). Thus, data from *PSP*'s Wave-Particle Correlator (WPC) could be an ideal tested for implementation of the PATCH algorithm that only requires the electric field in relatively high time-cadence and the particle times of arrival.

The WPC on *PSP* is a joint venture between the particle instrument suite, SWEAP (Kasper et al., 2016; Whittlesey et al., 2020), and the electromagnetic fields instrument suite, FIELDS (Bale et al., 2016), which interfaces with a DPU called the SWEAP Electronics Module (SWEM). Figure 6 shows a schematic of the interface cable that was placed between the particle electrostatic analyzer, SPAN, and fields instruments, FIELDS. The clock signal from FIELDS to SWEM provides a master clock so that FIELDS and SWEAP measurements can be made simultaneously with minimal time delays. Then, particle pulses are sent through a single channel from SWEM to FIELDS. Wave-particle correlations could be seen from up to 1 MHz, so we could potentially determine how energy is exchanged between electromagnetic fields and selected portions of the particle phase space density. Furthermore, the particle pulses can be selected from any combination of anodes from the electrostatic analyzers, so we can study both electron and ion scale kinetic physics. The primary goal for WPC implementation is to understand what causes heating in both particle populations.

The WPC enables the opportunity for refinement of the PATCH algorithm for application to real spacecraft data. However, we acknowledge that many key challenges exist for the practical implementation of the PATCH algorithm for the onboard computation of FPCs. These caveats include real-time determination of the appropriate frame of reference and magnetic-field-aligned coordinate system needed for time averaging the correlation. In addition, we must consider how to minimize the impact of instrumental effects, such as spacecraft charging, on the computed correlations. Once the PATCH concept is demonstrated to be realizable in pragmatic conditions, it could be further developed for onboard implementation on a future mission where exploring wave-particle interactions are of the primary science goals.

5. Summary

The technological advances of data acquisition onboard spacecraft far exceeds the rate of improvements in telemetry downlink bandwidths. Until Space-Earth telemetry methods (such as the Deep Space Network) become more developed and affordable, one solution to this excess data problem is to explore additional methods of compression. Data compression can take on many forms, but usually involves an element of averaging or redundancy removal in order to transmit less data with minimal loss in the quality of the original signal. This study demonstrated a proof-of-concept that energy transfer quantities from turbulent dissipation mechanisms may be pre-processed onboard for more optimal information downlinking capabilities.

Comprehending the dynamics and energetics of the entire cascade of turbulent energy from large scales, driven by violent events or instabilities, to small scales, eventually leading to plasma heat or some other form of energization, is the one of largest challenges in heliophysics. Understanding the nature of the dissipation mechanisms, that convert the turbulent energy into particle heat or an accelerated population of particles, represents one of the key aspects of this challenge. The FPC technique has the potential to diagnose and distinguish each of these mechanisms by constructing their characteristic velocity-space signature. This study extends the FPC technique for application to *in situ* discrete particle measurements, the Particle Arrival Time Correlation for Heliophysics (PATCH).

We developed PATCH as a new method of diagnosing energy transfer mechanisms onboard spacecraft based on time-tagging particles. We adapted the FPC concept to measure the net energy transfer by quantifying the statistical change in discrete particle counts over time. Utilizing spacecraft observations of discrete particle arrival times eliminates the need for calculating the phase-space bin-average of the distribution of particles. We instead showed that the distribution of the field measurements evaluated at the particle arrival times can yield the same information about the particle distribution function itself (see Appendix A for the full derivation from the Klimontovich–Dupree equation).

The PATCH algorithm was tested with synthetic spacecraft data produced by AstroGK, using the methodology of Verniero et al. (2021), by creating an artificial time series of particle counts using the numerically computed distribution function as the probability for counting a particle. The parallel electric field was then evaluated at those times; and a time correlation was performed and summed over velocity-space. Figure 3 presented a visualization of the statistical fluctuations of the new correlation as the typical number N of particles counted in a sampling time is increased. Note that N can be increased for a given instrument by increasing the sampling time per phase-space bin. Figure 3 showed that PATCH can qualitatively reproduce the velocity-space signature of ion Landau damping with a threshold of $N = 16$ particles for the typical single-bin particle count.

The quantitative analysis shown in Figures 4 and 5 demonstrates that the velocity-space integrated energy transfer rate $(dw_i(\mathbf{r}_0, t) / dt)_{E_{\parallel}}$ indeed converges to the “exact” value computed by the alternative FPC in *PSP* resolution, C'_{PSP} . However, to definitively determine the threshold number of particle counts needed to resolve the velocity-space signature of ion Landau damping, one must perform a larger number of statistical realizations of the PATCH method; and in turn, determine at which N the slope changes in Figure 5b. These changes in slope directly correspond to how the error scales as the number of particles counted per energy-bin increases. Future statistical studies with a range of solar wind conditions will enable this determination.

We have demonstrated, in this study, the possibility for a novel method of measuring energy transfer onboard spacecraft, with the aim to optimize scientific data return. PATCH utilizes discrete particle times of arrival along with simultaneous field measurements, yielding a simple algorithm that could revolutionize our understanding of wave-particle interactions, or other types of turbulent dissipation mechanisms. The kinetic theory re-imagined in Appendix A shows how to connect this new theory, in terms of particle number density, to existing ideas about energy transfer, in terms of distribution function measurements. The PATCH methodology is a crucial step toward implementing an onboard wave-particle correlator, which has been a multi-decadal challenge. With new technological capabilities available on *Parker Solar Probe*, the time is now.

Appendix A: Re-Imagining Kinetic Theory for Onboard FPCs

In this appendix, we show how to redefine the FPC technique using discrete particle counts. We then obtain an expression for the instantaneous rate of change in particle kinetic energy, using only information about the particle number density, rather than the distribution function, f_s . Note that the indices assigned to the various quantities defined in this appendix are independent of those in the main body of this study.

A1. Preliminary Definitions

Chapter 3 of Nicholson (1983) is based on the notion that point particles are described in a plasma existing in a 3D configuration-space \mathbf{r} , each with an orbit $\mathbf{r}(t)$. Likewise, the point particles exist in a 3D velocity-space \mathbf{v} with an orbit $\mathbf{v}(t)$. The two spaces combine to define the 6D (or 3D-3 V) phase-space (\mathbf{r}, \mathbf{v}) of the dynamical system of point particles. For each species s having N_0 particles in the system, the number density distribution N_s is

$$N_s(\mathbf{r}, \mathbf{v}, t) = \sum_i^{N_0} \delta[\mathbf{r} - \mathbf{r}_i(t)] \delta[\mathbf{v} - \mathbf{v}_i(t)] \quad (\text{A1})$$

The time derivative of the position orbit of particle i , denoted as an over-dot, is

$$\dot{\mathbf{r}}_i(t) = \mathbf{v}_i(t) \quad (\text{A2})$$

and the time derivative of the velocity orbit of particle i satisfies the Lorentz force equation

$$m_s \dot{\mathbf{v}}_i(t) = q_s \mathbf{E}^m[\mathbf{r}_i(t), t] + \frac{q_s}{c} \mathbf{v}_i(t) \times \mathbf{B}^m[\mathbf{r}_i(t), t] \quad (\text{A3})$$

where the superscript m denotes the self-consistently generated microscopic electric and magnetic fields produced by the point particles themselves, in addition to the externally applied fields. Maxwell's equations then describe the microscopic fields where the microscopic charge density is

$$\rho^m(\mathbf{x}, t) = \sum_{s,i} q_s \int d\mathbf{v} N_s(\mathbf{x}, \mathbf{v}, t) \quad (\text{A4})$$

and the microscopic current density is

$$\mathbf{J}^m(\mathbf{x}, t) = \sum_{s,i} q_s \int d\mathbf{v} \mathbf{v} N_s(\mathbf{x}, \mathbf{v}, t) \quad (\text{A5})$$

An exact description of the time evolution of the number density distribution of each species is then derived as

$$\frac{\partial N_s(\mathbf{r}, \mathbf{v}, t)}{\partial t} + \mathbf{v} \cdot \nabla_{\mathbf{r}} N_s + \frac{q_s}{m_s} \left(\mathbf{E}^m + \frac{\mathbf{v}}{c} \times \mathbf{B}^m \right) \cdot \nabla_{\mathbf{v}} N_s = 0 \quad (\text{A6})$$

known as the *Klimontovich–Dupree* equation (Dupree, 1963; Klimontovich, 1967). Together with Maxwell's equations, Equation A6 yields an exact description of the plasma (Nicholson, 1983).

A2. The Ensemble Average

In the next step of deriving the plasma kinetic equations, Nicholson (1983) introduces

$$f_s(\mathbf{x}, \mathbf{v}, t) = \langle N_s(\mathbf{x}, \mathbf{v}, t) \rangle \quad (\text{A7})$$

as the *ensemble average* over an “infinite number of realizations of the plasma,” as rigorously defined by Reif (1965). This distribution function is then substituted for N_s in the Klimontovich-Dupree Equation A6;

and the rest of kinetic plasma theory as we know it is derived from this critical stage (for example, the Vlasov equation is Equation A6 with f_s substituted for N_s). It was justified that this was done to deduce information about the *average* properties of the plasma (Nicholson, 1983).

The ensemble average represents the average number density of particles in all possible states of the system, which is an abstract mathematical notion to cast the spiky delta functions of $N_s(t)$ as a smooth distribution function. As suggested by V. I. Erofeev (2014), this notion of the ensemble average is not physically informative since it represents time evolutions of probabilities that do not naturally exist in the universe. In particular, these probabilities represent the statistics of all possibilities of any f_s realization, which is equivalent to saying that all f_s distribution functions are *indistinguishable*. This means that plasma physicists refer to f_s as if they were all the same. By definition of the ensemble average, indeed they are all the same; they are the average of every possible solution, which is certainly not observationally accessible knowledge. In a provocative article, V. V. Erofeev (2004) mentions in a footnote that, “as a first important system ensemble study we can mention [the] renown[ed] equation by Boltzmann. His concept of [a] distribution function supposes indirectly the substitution of a real mixture of discrete gas atoms by a continuous probabilistic ensemble of such mixtures. Boltzmann himself had no perception of this fact, although afterward he explicitly spoke about the desirability of substituting system ensembles for real systems (Boltzmann, 1896).”

Obtaining statistics about the number density of particles in any possible state obscures the specific physical problem at hand by including too much information that does not actually exist. To derive an actual physical result, substituting an unphysical f_s should be avoided (V. I. Erofeev, 2014). To smooth out the delta functions defined by N_s , V. I. Erofeev (2014) suggests that one should instead begin with the Klimontovich-Dupree equation and then take an appropriate phase-space or time average for the specific problem at hand. That way, the distributions will actually contain the much smaller subset of statistically relevant information to the physical problem, not the average statistics of every possible solution to the problem. For example, in deriving a three-wave interaction equation, V. I. Erofeev (1997) demonstrated how to avoid the ensemble average substitution by defining a distribution function in a way that accurately described the statistics of the physically observable situation.

A3. Onboard Correlation Derivation Using Kinetic Theory

In this section, we show how to circumvent the ensemble average to redefine the FPC technique with Equation A1, enabling an expression to be obtained for the rate of change in particle kinetic energy, using only information about the particle number density distribution, rather than the abstract and unphysical f_s . Ultimately, redefining the widely accepted approach of describing plasma evolution using the ensemble-averaged f and instead obtaining an expression in terms of particle counts (an observable quantity) will be more accessible information for instruments relevant for implementation of the PATCH method onboard spacecraft. Note that for derivation consistency with Klein and Howes (2016) and Howes et al. (2017), the Vlasov equation must also be redefined carefully (beyond the scope of this study) and will be left for future work.

Since our ultimate goal is to implement this technique onboard a spacecraft, we first restrict infinite 3D-3V phase-space to a finite 3D-3V phase-space instrumental measurement grid, $(\mathbf{r} \times \mathbf{v})_{\mathcal{G}}$. Note that the subscript, \mathcal{G} , suggests that the phase-space resolution of the particle instrument (ESA) is dependent on the geometric factor described by Equation 6 in Section 2.1. Then, $(\mathbf{r} \times \mathbf{v})_{\mathcal{G}}$ is comprised of approximately infinitesimal (smallest measurement bin size) 3D-3V phase-space volumes $\Delta \mathbf{r}_j \Delta \mathbf{v}_k$ centered at one phase-space coordinate, $(\mathbf{r}_j, \mathbf{v}_k)$, where

$$\sum_{j=1}^J \sum_{k=1}^K \Delta \mathbf{r}_j \Delta \mathbf{v}_k = (\mathbf{r} \times \mathbf{v})_{\mathcal{G}} \quad (\text{A8})$$

As defined, J and K correspond to the total number of spatial and velocity-space measurement bins on the instrument, respectively. Note here that in practice, the “spatial” measurement is a single point of observation, but we remain in a general framework to enable consistency with future technological advances. The “ \times ” notation refers to the Cartesian product, defining $(\mathbf{r} \times \mathbf{v})_{\mathcal{G}}$ as the set

$$(\mathbf{r} \times \mathbf{v})_G = \left\{ (\mathbf{r}_j, \mathbf{v}_k) \mid \mathbf{r}_j \in \Delta \mathbf{r}_j \quad \forall j \in J \text{ and } \mathbf{v}_k \in \Delta \mathbf{v}_k \quad \forall k \in K \right\}$$

Since each volume of phase-space is 3D-3V,

$$\mathbf{r}_j = (r_{1j}, r_{2j}, r_{3j}) \quad \forall j \in J \text{ and } \mathbf{v}_k = (v_{1k}, v_{2k}, v_{3k}) \quad \forall k \in K$$

Using Equation A1 for N_s , the microscopic kinetic energy of a collection of N_0 particles for each species, s , arriving at the detector aperture of the instrument is defined as

$$\begin{aligned} W_s^*(\mathbf{r}, \mathbf{v}, t) &= \int_{(\mathbf{r} \times \mathbf{v})_G} d^3 \mathbf{r} d^3 \mathbf{v} \frac{1}{2} m_s v^2 N_s \\ &= \int_{(\mathbf{r} \times \mathbf{v})_G} d^3 \mathbf{r} d^3 \mathbf{v} \frac{1}{2} m_s v^2 \sum_{i=1}^{N_0} \delta^3[\mathbf{r} - \mathbf{r}_i(t)] \delta^3[\mathbf{v} - \mathbf{v}_i(t)] \end{aligned} \quad (\text{A9})$$

To convert this to a phase-space energy density, define

$$w_s^*(\mathbf{r}_j, \mathbf{v}_k) \equiv \frac{W_s^*}{(\Delta \mathbf{r}_j \Delta \mathbf{v}_k)} \quad (\text{A10})$$

where $(\Delta \mathbf{r}_j \Delta \mathbf{v}_k)$ is one single volume element of phase space. We explicitly define the spatial limits of integration as

$$\int_{\Delta \mathbf{r}_j} d^3 \mathbf{r} = \int_{r_{1j} - \frac{\Delta r_{1j}}{2}}^{r_{1j} + \frac{\Delta r_{1j}}{2}} \int_{r_{2j} - \frac{\Delta r_{2j}}{2}}^{r_{2j} + \frac{\Delta r_{2j}}{2}} \int_{r_{3j} - \frac{\Delta r_{3j}}{2}}^{r_{3j} + \frac{\Delta r_{3j}}{2}} dr_1 dr_2 dr_3 \quad (\text{A11})$$

and the velocity-space integration limits as

$$\int_{\Delta \mathbf{v}_k} d^3 \mathbf{v} = \int_{v_{1k} - \frac{\Delta v_{1k}}{2}}^{v_{1k} + \frac{\Delta v_{1k}}{2}} \int_{v_{2k} - \frac{\Delta v_{2k}}{2}}^{v_{2k} + \frac{\Delta v_{2k}}{2}} \int_{v_{3k} - \frac{\Delta v_{3k}}{2}}^{v_{3k} + \frac{\Delta v_{3k}}{2}} dv_1 dv_2 dv_3 \quad (\text{A12})$$

By Equation A10, the microscopic kinetic energy within each approximately infinitesimal volume of phase-space for each species, s , is

$$w_s^* = \frac{1}{(\Delta \mathbf{r}_j \Delta \mathbf{v}_k)} \int_{\Delta \mathbf{r}_j} d^3 \mathbf{r} \int_{\Delta \mathbf{v}_k} d^3 \mathbf{v} \frac{1}{2} m_s v^2 \sum_{i=1}^{N_0} \delta^3[\mathbf{r} - \mathbf{r}_i(t)] \delta^3[\mathbf{v} - \mathbf{v}_i(t)] \quad (\text{A13})$$

Since we are in a finite space, we use the notion of a Dirac measure to test if a particle, p_i , is counted in $\Delta \mathbf{r}_j \Delta \mathbf{v}_k$:

$$\delta_{p_i}(\Delta \mathbf{r}_j \Delta \mathbf{v}_k) = \begin{cases} 1 & \text{if } p_i \in \Delta \mathbf{r}_j \Delta \mathbf{v}_k \\ 0 & \text{if } p_i \notin \Delta \mathbf{r}_j \Delta \mathbf{v}_k \end{cases} \quad (\text{A14})$$

This means the summation, over the δ -functions within a phase-space volume $\Delta \mathbf{r}_j \Delta \mathbf{v}_k$, commutes with (and is moved in front of) the integral when the upper summation limit is defined as the total number of particles, N_{tot} , counted within the 6D phase-space volume $\Delta \mathbf{r}_j \Delta \mathbf{v}_k$. Thus,

$$w_s^* = \frac{1}{(\Delta \mathbf{r}_j \Delta \mathbf{v}_k)} \sum_{i=1}^{N_{tot}} \int_{\Delta \mathbf{r}_j} d^3 \mathbf{r} \delta^3[\mathbf{r} - \mathbf{r}_i(t)] \int_{\Delta \mathbf{v}_k} d^3 \mathbf{v} \frac{1}{2} m_s v^2 \delta^3[\mathbf{v} - \mathbf{v}_i(t)] \quad (\text{A15})$$

Note the summation in Equation A15 is over the index i where $(\mathbf{r}_i(t), \mathbf{v}_i(t)) \in \Delta \mathbf{r}_j \times \Delta \mathbf{v}_k$.

Now, we restrict our coordinates to a single-point spacecraft measurement at the ESA detector aperture (depicted in Figure 1) with 2D surface area \mathbf{A} . Define $\Delta\mathbf{r}_p$ for some index $p \in J$ as the single 3D spatial volume element where a particle of species s , with velocity v_p , arrives at the aperture plane at some arrival time t_p , during a sampling time dt_p . In the summation over N_{tot} particles, the particle indexed by i with arrival time t_{pi} , occupies the fixed phase-space coordinate $(r_p(t_{pi}), v_p(t_{pi}))$ centered at $\Delta\mathbf{r}_p$, at an angle incident normal to the plane perpendicular to the detector aperture, within an approximately infinitesimal area $d\mathbf{A}_p$. We also assume only 1 particle passes through the aperture in the small local area $d\mathbf{A}_p$ at the instantaneous particle arrival time t_p , but multiple particles (indexed by i) can be counted in the sampling time dt_p .

For a particular r_1 and v_1 , we invoke the chain rule to observe $dr_1 = v_1 dt$. Let \mathbf{A} be the 2D surface area of the particle detector aperture such that $d\mathbf{A} = dr_2 \wedge dr_3$. Then, we redefine $\Delta\mathbf{r}_p = v_{1p} \Delta t_{1p} \Delta\mathbf{A}_{(2,3)}$, where the bin width, Δ , is the approximated infinitesimal width, d . Hence, $dr_{1p} = v_{1p} dt_{1p}$ and $d\mathbf{A}_{(2,3)p} = dr_{2p} \wedge dr_{3p}$. This means that

$$d^3\mathbf{r}_p = v_{1p} dt_{1p} d\mathbf{A}_{(2,3)p} \quad (\text{A16})$$

To avoid cumbersome notation, we will omit the subscripts identifying the dimension in the 3D coordinate $\mathbf{r}_p = (r_{1p}, r_{2p}, r_{3p})$, since they are already fixed and defined by Equation A16. Thus, the spatial integration coordinates from Equation A11 become

$$\int_{\Delta\mathbf{r}_p} d^3\mathbf{r}_p = \int_{t_p - \frac{\Delta t_p}{2}}^{t_p + \frac{\Delta t_p}{2}} \iint_{\mathbf{A}_p - \frac{\Delta\mathbf{A}_p}{2}}^{\mathbf{A}_p + \frac{\Delta\mathbf{A}_p}{2}} v_p dt_p d\mathbf{A}_p \quad (\text{A17})$$

Substituting Equation A17 for Equation A11 (and using the property $\delta(\alpha x) = \frac{\delta(x)}{\alpha}$), we find

$$\begin{aligned} & \int_{\Delta\mathbf{r}_p} d^3\mathbf{r}_p \delta^3[\mathbf{r}_p - \mathbf{r}_{pi}(t)] \\ &= \int_{t_p - \frac{\Delta t_p}{2}}^{t_p + \frac{\Delta t_p}{2}} \delta[v_p t_p - v_{pi} t_{pi}(t)] v_p dt_p \iint_{\mathbf{A}_p - \frac{\Delta\mathbf{A}_p}{2}}^{\mathbf{A}_p + \frac{\Delta\mathbf{A}_p}{2}} \delta^2[\mathbf{A}_p - \mathbf{A}_{pi}(t)] d\mathbf{A}_p \\ &= \int_{t_p - \frac{\Delta t_p}{2}}^{t_p + \frac{\Delta t_p}{2}} \delta[t_p - t_{pi}(t)] dt_p \end{aligned} \quad (\text{A18})$$

Substituting this result back into Equation A15,

$$w_s^* = \frac{1}{(\Delta\mathbf{r}_p \Delta\mathbf{v}_k)} \sum_{i=1}^{N_{\text{tot}}} \int_{t_p - \frac{\Delta t_p}{2}}^{t_p + \frac{\Delta t_p}{2}} \delta[t_p - t_{pi}(t)] dt_p \left[\frac{1}{2} m_s [\mathbf{v}_i(t)]^2 \right] \quad (\text{A19})$$

For each particle count indexed by i ,

$$t_{pi}(t) = \{t \in \Delta t_p \mid t = t_{pi}\} \quad (\text{A20})$$

so $t_{pi}(t) = t \mid_{\Delta t_p}$ and $[t_p - t_{pi}(t)] = 0$ when $t = t_{pi}$. Since the integration variable in Equation A19 is dt_p , the δ -functions are nonzero only when $t \in \Delta t_p$ for each particle indexed by i . Therefore, each term in the summation of Equation A19 is nonzero only at times $t = t_{pi}$, the instantaneous particle arrival times, meaning

$$w_s^* = \frac{1}{(\Delta\mathbf{r}_p \Delta\mathbf{v}_k)} \sum_{i=1}^{N_{\text{tot}}} \frac{1}{2} m_s [\mathbf{v}_i(t)]^2 \quad (\text{A21})$$

where $t \in \Delta t_p$ for each particle count indexed by i . The change in microscopic phase-space kinetic energy density is found by calculating the time derivative of Equation A21 to get

$$\frac{dw_s^*}{dt} = m_s \frac{1}{(\Delta \mathbf{r}_p \Delta \mathbf{v}_k)} \sum_{i=1}^{N_{tot}} \mathbf{v}_i(t) \cdot \dot{\mathbf{v}}_i(t)$$

where the over-dot implies the time derivative given by Equation A3. By substituting Equation A3 for $\dot{\mathbf{v}}_i(t)$, we get

$$\frac{dw_s^*}{dt} = \frac{1}{(\Delta \mathbf{r}_p \Delta \mathbf{v}_k)} \sum_{i=1}^{N_{tot}} q_s \mathbf{v}_i(t) \cdot \left[\mathbf{E}^m(\mathbf{r}_p(t), t) + \frac{q_s}{c} \mathbf{v}_i(t) \times \mathbf{B}^m(\mathbf{r}_p(t), t) \right] \quad (\text{A22})$$

Note that the magnetic field term vanishes since $\mathbf{v}_i(t) \cdot (\mathbf{v}_i(t) \times \mathbf{B}) = 0$. The term $\mathbf{v}_i(t) \in \Delta \mathbf{v}_k$ is interpreted as the 3D velocity orbit of particle i measured in the velocity-space bin $\Delta \mathbf{v}_k$. Thus, the summation terms in Equation A22 are only nonzero when $i = k$, so

$$\frac{dw_s^*}{dt} = \frac{1}{(\Delta \mathbf{r}_p \Delta \mathbf{v}_k)} \sum_{i=1}^{N_{tot}} q_s \mathbf{v}_k(t_{pi}) \cdot \mathbf{E}(\mathbf{r}_p(t_{pi}), t) \quad (\text{A23})$$

By definition of the set of particle arrival times given by A20, $\mathbf{v}_k(t)$ and $\mathbf{r}_p(t)$ are only nonzero when evaluated at $t = t_{pi}$.

The electric field term will have both a component contributing to oscillatory energy transfer and a component leading to net energy transfer. To isolate the component that leads to net energy transfer, the particle arrival time correlation over some correlation time interval, τ , must be longer than the particle sampling time dt_p , and chosen to be long enough so that the large-scale electric field contributing to the oscillating energy transfer averages approximately to 0. The FPC technique is hence redefined for onboard spacecraft implementation as the time-averaged rate of change of phase-space energy density, denoted here as the PATCH correlation C_τ^* :

$$C_\tau^* = \left\langle \frac{dw_s^*}{dt} \right\rangle_\tau = \frac{1}{\tau} \frac{1}{(\Delta \mathbf{r}_p \Delta \mathbf{v}_k)} \sum_{i=1}^{N_\tau} q_s \mathbf{v}_k(t_{pi}) \cdot \mathbf{E}(\mathbf{r}_p(t_{pi})) \quad (\text{A24})$$

where N_τ represents the total number of particles counted in a phase-space volume $\Delta \mathbf{r}_p \Delta \mathbf{v}_k$ over the suitable correlation time, τ , of Equation A23 that isolates the net energy transfer between the fields and particles.

This is consistent with the intuition prescribed in Section 2.2, with total number of particles, N_τ , given by Equation 9. Using Equation A24, the correlation (in a single phase-space bin $\Delta \mathbf{r}_p \Delta \mathbf{v}_p$) is

$$C_\tau^* = \frac{1}{\tau} \frac{1}{(\Delta \mathbf{r}_p \Delta \mathbf{v}_p)} \sum_{j=1}^{N_\tau} q_s \mathbf{v}_p \cdot \mathbf{E}(\mathbf{r}_p, t_j) \quad (\text{A25})$$

which is in agreement with Equation 13 per phase-phase bin. Note that \mathbf{v}_p was substituted for $\mathbf{v}_j(t_j) \in \Delta \mathbf{v}_p$ since this quantity is interpreted as the velocity (in spacecraft (E, Ω) coordinates) that each particle arrives in the bin $\Delta \mathbf{v}_p$. This velocity is fixed for each particle arrival time in local phase-space, since on the ESA, it corresponds to a fixed voltage difference and solid angle of rotation.

A4. Rate of Work Done on the Particles

We calculate the rate of work done on the particles (with species s) from the fields, $\mathbf{J} \cdot \mathbf{E}$, in a phase-space volume. From Equation A5,

$$\mathbf{J}(\mathbf{r}, t) = \sum_{s,t} q_s \int d^3 \mathbf{v} \mathbf{v} N_s(\mathbf{r}, \mathbf{v}, t) = \sum_{s,t=1}^{N_{tot}} q_s \int d^3 \mathbf{v} \delta^3[\mathbf{r} - \mathbf{r}_i(t)] \delta^3[\mathbf{v} - \mathbf{v}_i(t)] \quad (\text{A26})$$

Repeating the previous procedure in Section A3, we restrict the current density locally within a spatial volume $\Delta \mathbf{r}_p$ where particles arrive on the aperture, within in a single velocity-space bin $\Delta \mathbf{v}_k$. To obtain a

quantity for the work done on the particles in the phase-space volume $\Delta\mathbf{r}_p\Delta\mathbf{v}_k$, we compute the inner product of $\mathbf{J}(\mathbf{r},t)$ with the electric field in the spacecraft frame-of-reference (at the ESA aperture). Integrating over the locally defined phase-space volume, we get

$$\begin{aligned} & \mathbf{J} \cdot \mathbf{E} \Big|_{(\Delta\mathbf{r}_p\Delta\mathbf{v}_k)} \\ &= \sum_{s,i=1} q_s \frac{1}{(\Delta\mathbf{r}_p\Delta\mathbf{v}_k)} \int_{\Delta\mathbf{r}_p} d^3\mathbf{r} \mathbf{E}(\mathbf{r}_p(t),t) \delta^3[\mathbf{r} - \mathbf{r}_i(t)] \int_{\Delta\mathbf{v}_k} d^3\mathbf{v} \delta^3[\mathbf{v} - \mathbf{v}_i(t)] \\ &= \frac{1}{(\Delta\mathbf{r}_p\Delta\mathbf{v}_k)} \sum_{s,i=1}^{N_{tot}} q_s \int_{t_p - \frac{\Delta t_p}{2}}^{t_p + \frac{\Delta t_p}{2}} \mathbf{E}(\mathbf{r}_p(t),t) \delta[t_p - t_{pi}(t)] dt_p \cdot [\mathbf{v}_k(t)] \\ &= \frac{1}{(\Delta\mathbf{r}_p\Delta\mathbf{v}_k)} \sum_{s,i=1}^{N_{tot}} q_s \mathbf{E}(\mathbf{r}_p(t_{pi}),t) \cdot [\mathbf{v}_k(t)] \end{aligned} \quad (\text{A27})$$

where again, t_{pi} indicates the time of arrival for each particle indexed by i contained in the small phase-space volume $\Delta\mathbf{r}_p\Delta\mathbf{v}_k$. But since $t = t_{pi} \quad \forall t \in \mathbf{v}_k(t)$, Equation A27 becomes

$$\begin{aligned} \mathbf{J} \cdot \mathbf{E} \Big|_{(\Delta\mathbf{r}_p\Delta\mathbf{v}_k)} &= \frac{1}{(\Delta\mathbf{r}_p\Delta\mathbf{v}_k)} \sum_{s,i=1}^{N_{tot}} q_s \mathbf{v}_k(t_{pi}) \cdot \mathbf{E}(\mathbf{r}_p(t_{pi}),t) \\ &= \frac{dw_s^*}{dt} \end{aligned} \quad (\text{A28})$$

which matches Equation A23. Time-averaging Equation A28 over a long enough correlation interval, τ , to isolate the net transfer of energy by the electric field,

$$\begin{aligned} \left\langle \mathbf{J} \cdot \mathbf{E} \Big|_{(\Delta\mathbf{r}_p\Delta\mathbf{v}_k\tau)} \right\rangle &= \frac{1}{\tau} \frac{1}{\Delta\mathbf{r}_p\Delta\mathbf{v}_k} \sum_{s,i=1}^{N_\tau} q_s \mathbf{v}_k(t_{pi}) \cdot \mathbf{E}(\mathbf{r}_p(t_{pi})) \\ &= \left\langle \frac{dw_s^*}{dt} \right\rangle_\tau \\ &= C_\tau^* \end{aligned} \quad (\text{A29})$$

which verifies that C_τ^* is indeed measuring the work done on the particles by the electric field over a long-time average τ .

Data Availability Statement

Data were not used, nor created for this research.

Acknowledgments

J. L. Verniero was supported by the National Science Foundation Graduate Research Fellowship Program under Grant No. 1048957, the University of Iowa Graduate College Dissertation Completion Fellowship, and NASA Contract NNN06AA01C. G. G. Howes was supported by NASA Grants 80NSSC18K1217 and 80NSSC18K0643. K. G. Klein was supported by NASA Grant 80NSSC19K0912 and Contract NNN06AA01C.

References

- Bale, R., & Carbone, V. (2013). The solar wind as a turbulence laboratory. *Living Reviews in Solar Physics*, 10, 2. <https://doi.org/10.12942/lrsp-2013-2>
- Bale, S. D., Badman, S. T., Bonnell, J. W., Bowen, T. A., Burgess, D., Case, A. W., et al. (2019). Highly structured slow solar wind emerging from an equatorial coronal hole. *Nature*, 576(7786), 237–242. <https://doi.org/10.1038/s41586-019-1818-7>
- Bale, S. D., Goetz, K., Harvey, P. R., Turin, P., Bonnell, J. W., Dudok de Wit, T., et al. (2016). The FIELDS instrument suite for solar probe plus. *Space Science Reviews*, 204, 49–82. <https://doi.org/10.1007/s11214-016-0244-5>
- Belcher, J. W., & Davis, L. (1971). Large-amplitude Alfvén waves in the interplanetary medium, 2. *Journal of Geophysical Research*, 76, 3534–3563. <https://doi.org/10.1029/ja076i016p03534>
- Boltzmann, L. (1896). *Vorlesungen über gastheorie: Th. Theorie des gase mit einatomigen molekülen, deren dimensionen gegen die mittlere weglänge verschwinden*. Retrieved from <https://books.google.com/books?id=iZcAAAAAMAAJ>
- Bowen, T. A., Mallet, A., Huang, J., Klein, K. G., Malaspina, D. M., Stevens, M., et al. (2020). Ion-scale electromagnetic waves in the inner heliosphere. *The Astrophysical Journal Supplement Series*, 246(2), 66. <https://doi.org/10.3847/1538-4365/ab6c65>
- Carlson, C. W., Curtis, D. W., Paschmann, G., & Michel, W. (1982). An instrument for rapidly measuring plasma distribution functions with high resolution. *Advances in Space Research*, 2(7), 67–70. Retrieved from <http://www.sciencedirect.com/science/article/pii/027311778290151X>
- Chandran, B. D. G. (2010). Alfvén-wave turbulence and perpendicular ion temperatures in coronal holes. *Acta Pathologica Japonica*, 720, 548–554. <https://doi.org/10.1088/0004-637X/720/1/548>
- Chandran, B. D. G., Li, B., Rogers, B. N., Quataert, E., & Germaschewski, K. (2010). Perpendicular ion heating by low-frequency Alfvén-wave turbulence in the solar wind. *Acta Pathologica Japonica*, 720, 503–515. <https://doi.org/10.1088/0004-637X/720/1/503>

- Chen, C. H. K., Klein, K. G., & Howes, G. G. (2019). Evidence for electron Landau damping in space plasma turbulence. *Nature Communications*, 10(1), 740. <https://doi.org/10.1038/s41467-019-08435-3>
- Chen, L., Lin, Z., & White, R. (2001). On resonant heating below the cyclotron frequency. *Physics of Plasmas*, 8, 4713–4716. <https://doi.org/10.1063/1.1406939>
- Dmitruk, P., Matthaeus, W. H., & Seenu, N. (2004). Test particle energization by current sheets and nonuniform fields in magnetohydrodynamic turbulence. *Acta Pathologica Japonica*, 617, 667–679. <https://doi.org/10.1086/425301>
- Dupree, T. H. (1963). Kinetic theory of plasma and the electromagnetic field. *Physics of Fluids*, 6(12). <https://doi.org/10.1063/1.1711014>
- Ergun, R. E., Carlson, C. W., McFadden, J. P., Clemmons, J. H., & Boehm, M. H. (1991). Langmuir wave growth and electron bunching: Results from a wave-particle correlator. *Journal of Geophysical Research*, 96, 225–238. <https://doi.org/10.1029/90JA01596>
- Erofeev, V. (2004). *Rational paradigm of plasma physics*. 12th International Congress on Plasma Physics, 25–29 October 2004, Nice (France) Retrieved from <https://hal.archives-ouvertes.fr/hal-00001721>
- Erofeev, V. I. (1997). Derivation of an equation for three-wave interactions based on the Klimontovich-Dupree equation. *Journal of Plasma Physics*, 57(2), 273–298. <https://doi.org/10.1017/S0022377896004990>
- Erofeev, V. I. (2014). High-informative version of nonlinear transformation of Langmuir waves to electromagnetic waves. *Journal of Plasma Physics*, 80(2), 289–318. <https://doi.org/10.1017/S002237781300127X>
- Fox, N. J., Velli, M. C., Bale, S. D., Decker, R., Driesman, A., Howard, R. A., et al. (2016). The solar probe plus mission: Humanity's first visit to our star. *Space Science Reviews*, 204, 7–48. <https://doi.org/10.1007/s11214-015-0211-6>
- Fukuhara, H., Kojima, H., Ueda, Y., Omura, Y., Katoh, Y., & Yamakawa, H. (2009). A new instrument for the study of wave-particle interactions in space: One-chip wave-particle interaction analyzer. *Earth, Planets and Space*, 61, 765–778. <https://doi.org/10.1186/bf03353183>
- Gough, M. P., Burke, W. J., Hardy, D. A., Huang, C. Y., Gentile, L. C., Rubin, A. G., et al. (1998). Megahertz electron modulations during TSS 1R. *Geophysical Research Letters*, 25, 441–444. <https://doi.org/10.1029/97GL03002>
- Gough, M. P., Christiansen, P. J., & Wilhelm, K. (1990). Auroral beam-plasma interactions: Particle correlator investigations. *Journal of Geophysical Research*, 95, 12287–12294. <https://doi.org/10.1029/JA095iA08p12287>
- Gough, M. P., Hardy, D. A., Burke, W. J., Oberhardt, M. R., Gentile, L. C., Huang, C. Y., et al. (1997). Heating and low-frequency modulation of electrons observed during electron beam operations on TSS 1. *Journal of Geophysical Research*, 102, 17335–17357. <https://doi.org/10.1029/97JA00801>
- Gough, M. P., Hardy, D. A., Oberhardt, M. R., Burke, W. J., Gentile, L. C., McNeil, B., et al. (1995). Correlator measurements of megahertz wave-particle interactions during electron beam operations on STS. *Journal of Geophysical Research*, 100, 21561–21575. <https://doi.org/10.1029/95JA00679>
- Gough, M. P., Hardy, D. A., Oberhardt, M. R., Burke, W. J., Gentile, L. C., Thompson, D. C., et al. (1998). Spree measurements of wave-particle interactions generated by the electron guns on TSS-1 and TSS-1R. *Advances in Space Research*, 21, 729–733. [https://doi.org/10.1016/S0273-1177\(97\)01013-2](https://doi.org/10.1016/S0273-1177(97)01013-2)
- Gough, M. P., & Urban, A. (1983). Auroral beam/plasma interaction observed directly. *Planetary and Space Science*, 31, 875–883.
- Howes, G. G., Klein, K. G., & Li, T. C. (2017). Diagnosing collisionless energy transfer using field-particle correlations: Vlasov-Poisson plasmas. *Journal of Plasma Physics*, 83(1), 705830102. <https://doi.org/10.1017/S0022377816001197>
- Howes, G. G., & Nielson, K. D. (2013). Alfvén wave collisions, the fundamental building block of plasma turbulence. I. Asymptotic solution. *Physics of Plasmas*, 20(7), 072302. <https://doi.org/10.1063/1.4812805>
- Johnson, J. R., & Cheng, C. Z. (2001). Stochastic ion heating at the magnetopause due to kinetic Alfvén waves. *Geophysical Research Letters*, 28, 4421–4424. <https://doi.org/10.1029/2001GL013509>
- Karimabadi, H., Roytershteyn, V., Wan, M., Matthaeus, W. H., Daughton, W., Wu, P., et al. (2013). Coherent structures, intermittent turbulence, and dissipation in high-temperature plasmas. *Physics of Plasmas*, 20(1), 012303. <https://doi.org/10.1063/1.4773205>
- Kasper, J. C., Abiad, R., Austin, G., Balat-Pichelin, M., Bale, S. D., Belcher, J. W., et al. (2016). Solar Wind Electrons Alphas and Protons (SWEAP) investigation: Design of the solar wind and coronal plasma instrument suite for solar probe plus. *Space Science Reviews*, 204, 131–186. <https://doi.org/10.1007/s11214-015-0206-3>
- Katoh, Y., Kitahara, M., Kojima, H., Omura, Y., Kasahara, S., Hirahara, M., et al. (2013). Significance of wave-particle interaction analyzer for direct measurements of nonlinear wave-particle interactions. *Annales Geophysicae*, 31(3), 503–512. <https://doi.org/10.5194/angeo-31-503-2013>
- Kitamura, N., Kitahara, M., Shoji, M., Miyoshi, Y., Hasegawa, H., Nakamura, S., et al. (2018). Direct measurements of two-way wave-particle energy transfer in a collisionless space plasma. *Science*, 361, 1000–1003. <https://doi.org/10.1126/science.aap8730>
- Klein, K. G., & Howes, G. G. (2016). Measuring collisionless damping in heliospheric plasmas using field-particle correlations. *Acta Pathologica Japonica*, 826, L30. <https://doi.org/10.3847/2041-8205/826/2/L30>
- Klein, K. G., Howes, G. G., & TenBarge, J. M. (2017). Diagnosing collisionless energy transfer using field-particle correlations: Gyrokinetic turbulence. *Journal of Plasma Physics*, 83(4), 535830401. <https://doi.org/10.1017/S0022377817000563>
- Kletzing, C. A., Bounds, S. R., LaBelle, J., & Samara, M. (2005). Observation of the reactive component of Langmuir wave phase-bunched electrons. *Geophysical Research Letters*, 32, L05106. <https://doi.org/10.1029/2004GL021175>
- Klimontovich, Y. L. (1967). *The Statistical Theory of Non-equilibrium Processes in a Plasma* (Translated by H.S.H. Massey and O.M. Blunn). M.I.T. Press.
- Kraichnan, R. H. (1965). Inertial-range spectrum of hydromagnetic turbulence. *Physics of Fluids*, 8, 1385–1387. <https://doi.org/10.1063/1.1761412>
- Lichko, E., & Egedal, J. (2020). Magnetic pumping model for energizing superthermal particles applied to observations of the Earth's bow shock. *Nature Communications*, 11, 2942. <https://doi.org/10.1038/s41467-020-16660-4>
- Lichko, E., Egedal, J., Daughton, W., & Kasper, J. (2017). Magnetic pumping as a source of particle heating and power-law distributions in the solar wind. *Acta Pathologica Japonica*, 850, L28. <https://doi.org/10.3847/2041-8213/aa9a33>
- Lin, R. P., Anderson, K. A., Ashford, S., Carlson, C., Curtis, D., Ergun, R., et al. (1995). A three-dimensional plasma and energetic particle investigation for the wind spacecraft. *Space Science Reviews*, 71, 125–153. <https://doi.org/10.1007/BF00751328>
- Malaspina, D. M., Halekas, J., Berčić, L., Larson, D., Whittlesey, P., Bale, S. D., et al. (2020). Plasma waves near the electron cyclotron frequency in the near-sun solar wind. *The Astrophysical Journal Supplement Series*, 246(2), 21. <https://doi.org/10.3847/1538-4365/ab4c3b>
- Matthaeus, W. H., & Montgomery, D. (1980). Selective decay hypothesis at high mechanical and magnetic Reynolds numbers*. *Annals of the New York Academy of Sciences*, 357, 203–222. <https://doi.org/10.1111/j.1749-6632.1980.tb29687.x>
- Nicholson, D. (1983). *Introduction to Plasma Theory*. Wiley. Retrieved from <https://books.google.com/books?id=fyRRAAAMAAl>
- Numata, R., Howes, G. G., Tatsuno, T., Barnes, M., & Dorland, W. (2010). AstroGK: Astrophysical gyrokinetics code. *Journal of Computational Physics*, 229, 9347. <https://doi.org/10.1016/j.jcp.2010.09.006>

- Osman, K. T., Kiyani, K. H., Chapman, S. C., & Hnat, B. (2014). Anisotropic intermittency of magnetohydrodynamic turbulence. *Acta Pathologica Japonica*, 783, L27. <https://doi.org/10.1088/2041-8205/783/2/L27>
- Osman, K. T., Matthaeus, W. H., Gosling, J. T., Greco, A., Servidio, S., Hnat, B., et al. (2014). Magnetic reconnection and intermittent turbulence in the solar wind. *Physical Review Letters*, 112(21), 215002. <https://doi.org/10.1103/PhysRevLett.112.215002>
- Reif, F. F. (1965). *Fundamentals of Statistical and Thermal Physics*. McGraw-Hill.
- Rubin, A. G., Burke, W. J., Gough, M. P., Machuzak, J. S., Gentile, L. C., Huang, C. Y., et al. (1999). Beam-induced electron modulations observed during TSS 1R. *Journal of Geophysical Research*, 104, 17251–17262. <https://doi.org/10.1029/1999JA900127>
- Spiger, R. J., Murphree, J. S., Anderson, H. R., & Loewenstein, R. F. (1976). Modulation of auroral electron fluxes in the frequency range 50 kHz to 10 MHz. *Journal of Geophysical Research*, 81, 1269–1278. <https://doi.org/10.1029/JA081i007p01269>
- Spiger, R. J., Oehme, D., Loewenstein, R. F., Murphree, J., Anderson, H. R., & Anderson, R. (1974). A detector for high frequency modulation in auroral particle fluxes. *Review of Scientific Instruments*, 45, 1214–1220. <https://doi.org/10.1063/1.1686462>
- Vech, D., Klein, K. G., & Kasper, J. C. (2017). Nature of stochastic ion heating in the solar wind: testing the dependence on plasma beta and turbulence amplitude. *Acta Pathologica Japonica*, 850, L11. <https://doi.org/10.3847/2041-8213/aa9887>
- Verniero, J. L., & Howes, G. G. (2018). The Alfvénic nature of energy transfer mediation in localized, strongly nonlinear Alfvén wavepacket collisions. *Journal of Plasma Physics*, 84(1), 905840109. <https://doi.org/10.1017/S0022377818000090>
- Verniero, J. L., Howes, G. G., & Klein, K. G. (2018). Nonlinear energy transfer and current sheet development in localized Alfvén wavepacket collisions in the strong turbulence limit. *Journal of Plasma Physics*, 84(1), 905840103. <https://doi.org/10.1017/S0022377817001003>
- Verniero, J. L., Howes, G. G., Stewart, D. E., & Klein, K. G. (2021). Determining threshold instrumental resolutions for resolving the velocity-space signature of ion Landau damping. *Journal of Geophysical Research: Space Physics*, 126, e2020JA028361. <https://doi.org/10.1029/2020JA028361>
- Verniero, J. L., Larson, D. E., Livi, R., Rahmati, A., McManus, M. D., Pyakurel, P. S., et al. (2020). Parker solar probe observations of proton beams simultaneous with ion-scale waves. *The Astrophysical Journal Supplement Series*, 248(1), 5. <https://doi.org/10.3847/1538-4365/ab86af>
- Verscharen, D., Klein, K. G., & Maruca, B. A. (2019). The multi-scale nature of the solar wind. *Living Reviews in Solar Physics*, 16(1), 5. <https://doi.org/10.1007/s41116-019-0021-0>
- Whittlesey, P. L., Larson, D. E., Kasper, J. C., Halekas, J., Abatcha, M., Abiad, R., et al. (2020). The Solar Probe ANalyzers-Electrons on the Parker Solar Probe. *The Astrophysical Journal Supplement Series*, 246(2), 74. <https://doi.org/10.3847/1538-4365/ab7370>
- Woolliscroft, L. J. C., Alleyne, H. S. C., St C. Alleyne, H., Dunford, C. M., Sumner, A., Thompson, J. A., et al. (1997). The digital wave-processing experiment on cluster. *Space Science Reviews*, 79, 209–231. https://doi.org/10.1023/A:100491421186610.1007/978-94-011-5666-0_9
- Zhdankin, V., Boldyrev, S., Perez, J. C., & Tobias, S. M. (2014). Energy dissipation in magnetohydrodynamic turbulence: coherent structures or “nanoflares”? *Acta Pathologica Japonica*, 795, 127. <https://doi.org/10.1088/0004-637X/795/2/127>
- Zhdankin, V., Uzdensky, D. A., Perez, J. C., & Boldyrev, S. (2013). Statistical analysis of current sheets in three-dimensional magnetohydrodynamic turbulence. *Acta Pathologica Japonica*, 771, 124. <https://doi.org/10.1088/0004-637X/771/2/124>